Available online at www.sciencedirect.com
ScienceDirect

Trans. Nonferrous Met. Soc. China 22(2012) 391−397

Transactions of Nonferrous Metals Society of China

www.tnmsc.cn

Effect of forced lamina flow on microsegregation simulated by phase field method quantitatively

WANG Jun-wei[1], WANG Zhi-ping[1, 2], LU Yang[1, 2], ZHU Chang-sheng[1, 3], FENG Li[1], XIAO Rong-zhen[1]

1. State Key Laboratory of Gansu Advanced Nonferrous Metal Materials, Lanzhou University of Technology, Lanzhou 730050, China;
2. Research Center of Gansu Nonferrous Metal Materials and Composite Materials Engineering, Lanzhou 730050, China;
3. CAD Center, Lanzhou University of Technology, Lanzhou 730050, China

Received 14 March 2011; accepted 18 June 2011

Abstract: The influence of supercooled melt forced lamina flow on microsegregation was investigated. The concentration distribution at solid−liquid boundary of binary alloy Ni−Cu was simulated using phase field model coupled with flow field. The microsegregation, concentration maximum value, boundary thickness of concentration near upstream dendrite and normal to flow dendrite, and downstream dendrite were studied quantitatively in the case of forced lamia flow. The simulation results show that solute field and flow field interact complexly. Compared with melt without flow, in front of upstream dendrite tip, the concentration boundary thickness is the lowest and the concentration maximum value is the smallest for melt with flow. However, in front of downstream dendrite tip, the results are just the opposite. The zone of poor Cu in upstream dendrite where is the most severely microsegregation and shrinkage cavity is wider and the concentration is lower for melt with flow than that without flow.

Key words: computer simulation; phase field method; solidification; forced lamina flow; microsegregation; solute redistribution; shrinkage cavity

1 Introduction

Casting performance is influenced by the solidification microstructure of alloys [1]. Decrease in shrinkage cavity is one of the hot spots at present [2, 3]. There is no doubt that convection happens in the supercooled melt during solidification [4, 5]. Phase field method based on Ginzburg−Landau theory has been used by domestic and foreign scholars to research solidification microstructure under the effect of convection [6−8]. Great achievements are obtained on pure material to alloy [9−11], isothermal to non-isothermal [12−14], supercooled melt without flow to that with flow [15−18] and so on [19−21]. However, these studies focused on qualitative study of non-symmetrical dendritic morphology. Some researchers referred to solute distribution asymmetry and solute rejection phenomenon, but they did not relate to the concentration boundary layer thickness features in front of upstream dendrite, normal to flow dendrite and downstream dendrite in detail. Maximal concentration values in front of 3 directions of dendrite were also not contrasted [2, 11, 12, 17].

Taking binary alloy Ni−0.408Cu for an example, solidification microstructure under the effect of supercooled melt forced lamina flow during non-isothermal and uniform crystal phase transition is studied by phase field method. The method is based on sola-phase field model (S-PFM) idea of pure material and coupled with solute field control equation [22]. Flow control equations are solved by algorithm Sola method [23]. In this study, the effect of supercooled melt forced lamina flow under concentration boundary layer thickness and max concentration values in front of 3-direction dendrite (upstream dendrite, normal to flow dendrite and downstream dendrite) were studied quantitatively in detail. The microsegregation formation mechanisms during alloy solidification were investigated by computer simulation method.

Foundation item: Project (10964004) supported by the National Natural Science Foundation of China; Project (20070731001) supported by Research Fund for the Doctoral Program of China; Project (096RJZA104) supported by the Natural Science Foundation of Gansu Province, China
Corresponding author: WANG Zhi-ping; Tel: +86-931-2973690; E-mail: wangzp@lut.cn
DOI: 10.1016/S1003-6326(11)61189-8

2 Mathematical model

The flow equations were solved numerically using algorithm Sola method and the position of freeze dendrite was fixed. Detailed process can be found in Ref. [22]. Supercooled melt forced lamina flow has an effect not only on temperature field but also on solute field. So, a 2D mathematical model was made by coupled solute field control equation of binary alloy with phase field equations of pure material for melt with flow filed. The 2D mathematical model is shown as:

$$\frac{\partial \phi}{\partial t}=\left(\frac{(1-c)\left(T_{\mathrm{m}}^{\mathrm{A}}\right)^2\sigma_{\mathrm{A}}}{6\sqrt{2}L_{\mathrm{A}}\lambda}+\frac{c\left(T_{\mathrm{m}}^{\mathrm{B}}\right)^2\sigma_{\mathrm{B}}}{6\sqrt{2}L_{\mathrm{B}}\lambda}\right)\cdot \left\{\nabla\left(w(\theta)^2\nabla\phi\right)-\left[h'(\phi)((1-c)H_{\mathrm{A}}+cH_{\mathrm{B}})+ g'(\phi)\left(\frac{3(1-c)\sigma_{\mathrm{A}}}{\sqrt{2}T_{\mathrm{m}}^{\mathrm{A}}\delta}+\frac{3c\sigma_{\mathrm{B}}}{\sqrt{2}T_{\mathrm{m}}^{\mathrm{B}}\delta}\right)\right](1+9r16g(\phi))\right\} \quad (1)$$

$$\frac{\partial T}{\partial t}+(1-\phi)\boldsymbol{u}\nabla T=D_{\mathrm{T}}\nabla^2 T+\frac{\partial}{\partial t}\left\{\frac{(1-h(\phi))}{c_{\mathrm{p}}}\cdot \left[(1-c)L_{\mathrm{A}}+cL_{\mathrm{B}}\right]\right\} \quad (2)$$

$$\frac{\partial c}{\partial t}=-\nabla\left\{D_{\mathrm{c}}c(1-c)\frac{v_{\mathrm{m}}}{R}\nabla(\delta^2\nabla^2 c)+ D_{\mathrm{c}}c(1-c)\frac{v_{\mathrm{m}}}{R}\left[P_{\mathrm{A}}(\phi,T)-P_{\mathrm{B}}(\phi,T)\right]\nabla\phi- D_{\mathrm{c}}c(1-c)\frac{v_{\mathrm{m}}}{TR}\left[\frac{g(\phi)}{T}(L^{\mathrm{A}}-L^{\mathrm{B}})+(c_p^{\mathrm{A}}-c_p^{\mathrm{B}})\right]\cdot \nabla T-D_{\mathrm{c}}\nabla c\right\}-\phi\boldsymbol{u}\cdot\nabla c \quad (3)$$

$$\mathrm{div}\boldsymbol{u}=0 \quad (4)$$

$$\begin{cases}\dfrac{\partial u}{\partial t}+u\dfrac{\partial u}{\partial x}+v\dfrac{\partial u}{\partial y}=-\dfrac{1}{\rho}\dfrac{\partial p}{\partial x}+g_x+\upsilon(\dfrac{\partial^2 u}{\partial x^2}+\dfrac{\partial^2 u}{\partial y^2})\\[2mm] \dfrac{\partial v}{\partial t}+u\dfrac{\partial v}{\partial x}+v\dfrac{\partial v}{\partial y}=-\dfrac{1}{\rho}\dfrac{\partial p}{\partial y}+g_y+\upsilon(\dfrac{\partial^2 v}{\partial x^2}+\dfrac{\partial^2 v}{\partial y^2})\end{cases} \quad (5)$$

where Eqs. (1), (2) and (3) are the phase field control equation, energy conservation equation of pure material which is coupled with melt flow and solute field control equation, respectively. Equations.(4) and (5) are conservation equations of mass and momentum of viscous incompressible flow, respectively. Phase-field variable Φ=1 and Φ=0 refer to solid phase and bulk liquid, and the number of Φ=0−1 refer to solid−liquid interface. c, λ, δ and c_p are the solute concentration, coupling constant, interface thickness and specific heat capacity, respectively; D_{T} and D_{c} are the thermal diffusivity and solute diffusivity, respectively; T_{m}, σ and L superscripted or subscripted with A and B are the melting temperature, interface energy and crystallization latent heat of A and B, respectively; T, R, v_{m}, ρ and υ are the temperature (K), gas constant, volume of one mole (m^3/mol), density ($\mathrm{kg/m}^3$) and kinematic viscosity coefficient (m^2/s), respectively. $h(\phi)=\phi^3(10-15\phi+6\phi^2)$ is a construct function, which monotonely increases with increasing ϕ from 0 to 1; $g(\phi)=\phi^2(1-\phi)^2$ is a double-well potential function; $w(\theta)$ is a parameter referring to interface thickness; Supercooled melt flow velocity $\boldsymbol{u}=ui+vj$. $P_{\mathrm{A}}(\phi, T)$ and $P_{\mathrm{B}}(\phi, T)$ in Eq.(3) are calculated as:

$$\begin{cases}P_{\mathrm{A}}=h'(\phi)L_{\mathrm{A}}\left(\dfrac{1}{T}-\dfrac{1}{T_{\mathrm{m}}^{\mathrm{A}}}\right)+g'(\phi)\dfrac{3\sigma_{\mathrm{A}}}{\sqrt{2}T_{\mathrm{m}}^{\mathrm{A}}\delta}\\[2mm] P_{\mathrm{B}}=h'(\phi)L^{\mathrm{B}}\left(\dfrac{1}{T}-\dfrac{1}{T_{\mathrm{m}}^{\mathrm{A}}}\right)+g'(\phi)\dfrac{3\sigma_{\mathrm{B}}}{\sqrt{2}T_{\mathrm{m}}^{\mathrm{B}}\delta}\end{cases} \quad (6)$$

3 Numerical issues

Program is made in C language on VC++6.0 platform. The initial dendrite is 1 sphericity (radius=R), which is fixed in the centre of simulation zone. The initial pressure and degree of supercooling are p and ΔT, respectively. The initial condition is shown as:

$$\begin{cases}x^2+y^2\le R^2, \phi=1, \Delta T=0, \boldsymbol{u}=0, v=0, p=0\\ x^2+y^2> R^2, \phi=0, \Delta T=20.5\ \mathrm{K}, u=1.3\ \mathrm{m/s}, v=0, p=0\end{cases} \quad (7)$$

The Zero—Nuemnna adiabatic boundary condition is used. Phase field variable φ, temperature T and solute concentration c on the normal direction of solid−liquid interface $\boldsymbol{n}$ are expressed as:

$$\frac{\partial\phi}{\partial\boldsymbol{n}}=0,\ \frac{\partial T}{\partial\boldsymbol{n}}=0,\ \frac{\partial c}{\partial\boldsymbol{n}}=0 \quad (8)$$

Double staggered grid is used. φ and p are placed on one piece of grid and $\boldsymbol{u}$ is on another piece of grid, u and v are placed on north and east boundaries, respectively.

Phase field control equation is solved by the explicit difference method. $\nabla(w(\theta)^2\nabla\phi)$ in Eq.(1) is expanded as:

$$\nabla(w(\theta)^2\nabla\phi)=w_0^2\nabla[a_0^2(\boldsymbol{n})\nabla\phi]- \frac{\partial}{\partial x}\left[w_0^2 a_{\mathrm{s}}(\boldsymbol{n})a_{\mathrm{s}}'(\boldsymbol{n})\frac{\partial\phi}{\partial y}\right]+\frac{\partial}{\partial y}\left[w_0^2 a_{\mathrm{s}}(\boldsymbol{n})a_{\mathrm{s}}'(\boldsymbol{n})\frac{\partial\phi}{\partial x}\right] \quad (9)$$

where $a_{\mathrm{s}}(\boldsymbol{n})$ is the anisotropic parameter; $a_{\mathrm{s}}(\boldsymbol{\theta})=1+\varepsilon\cos 4\theta$ where ε is the anisotropy strength of the surface energy and θ is the angle between interfacial and x-axis. The difference of temperature equation between couples with flow and without flow is $(1-\phi)\boldsymbol{u}\nabla T$, which is expanded as:

$$(1-\phi)\boldsymbol{u}\nabla T=(1-\phi)(ui+vj)\left(\frac{\partial T}{\partial x}i+\frac{\partial T}{\partial y}j\right)$$
$$=(1-\phi)\left(u\frac{\partial T}{\partial x}+v\frac{\partial T}{\partial y}\right) \quad (10)$$

The mole fraction of Cu is 0.408 in Ni−Cu alloy is solute. Binary alloy Ni−0.408Cu is simulation material in this study. The material parameters and practical calculation parameters are listed in Table 1.

4 Results and discussion

Figures 1(a), (b) and (c) show the binary alloy phase field, temperature filed and solute filed when supercooled melt flow velocity is 0 at t=34200Δt, respectively. When the melt flow velocity is 1.3 m/s,

Table 1 Material parameters of Ni−0.408Cu and practical calculation parameters

Material	T_m/K	L/(J·cm^{-3})	V_m/(cm^3·mol^{-1})	σ/(10^{-5}J·cm^{-2})	β/(cm·K^{-1}·s^{-1})	Δx, Δy/cm	
Ni	1728	2350	7.0	3.75	0.33	2.4×10^{-6}	
Cu	1358	1728	7.8	2.8	0.36		
Material	δ/cm	Δt/s	D_s/(cm·s^{-1})	D_l/(cm·s^{-1})	ΔT/K	ε	ω
Ni-0.408Cu	4.5×10^{-6}	1.1×10^{-8}	1×10^{-9}	1×10^{-5}	20.5	0.06	0.001

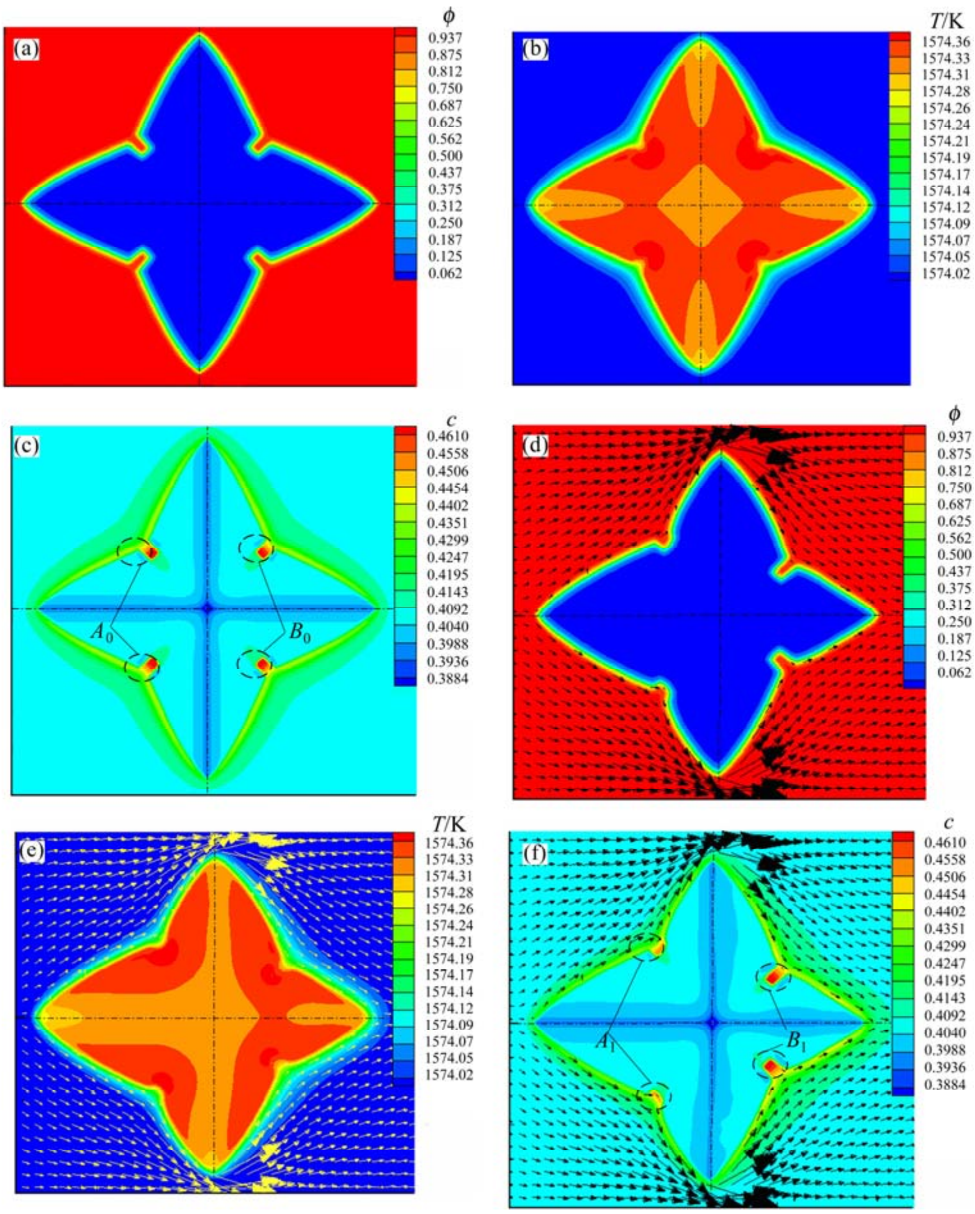

Fig. 1 Phase filed (a, b), temperature field (b, e) and solute-flow field (c, f) at u=0 (a, b, c) and 1.3 m/s (d, e, f) at t=34200Δt

phase field, temperature filed and solute-flow filed are shown in Figs. 1(d), (e) and (f). Arrow direction and length represent the melt particles flow direction and flow velocity value, respectively. The longer the arrow line is and the wider the arrow width is, the higher the melt flow velocity is, and vice versa. By comparing Fig. 1(a) with Fig. 1(d), Fig. 1(b) with Fig. 1(e) and Fig. 1(c) with Fig. 1(f), it can be found that symmetry morphology, temperature filed and solute filed about vertical axis of concentration distribution are changed by melt flow. What is more, melt is flowing around fixed dendrite. Flow velocity becomes higher at upper and lower boundaries. This is because the cross-section width of melt flow becomes smaller, but the melt inflow velocity is invariant. The area of low temperature zone in upstream dendrite arm increases because of severe thermal convection. In all, there is an interaction between melt flow state and dendrite growth process.

Cu atoms enrich and the concentration increases between two adjacent dendrites because of solute redistribution, as shown in regions A_0 and B_0 in Fig. 1(c). For melt with flow, as shown in Fig. 1(f), Cu enrichment reduces (region A_1) at upstream dendrite because strong convection takes Cu atoms away. So, corresponding liquidus temperature does not decrease very much and it relieves the shrinkage cavity trend. However, Cu enrichment increases sharply at downstream dendrite (region B_1) and its molar fraction increases from 0.458 to 0.461 for melt without flow (region B_0). Cu is precipitated from solid phase and comes from upstream with melt flow, and the convection strength is very weak. At downstream dendrite, liquidus temperature reduces sharply and there (region B_1) is the last freeze zone, and shrinkage cavity appears in region B_1 easily. If there is eutectic phase transition during solidification, eutectic structure appears when solute concentration equals eutectic concentration. But there is no eutectic structure because there is no eutectic phase transition during the solidification of Cu−Ni alloy.

The thickness of concentration boundary layer and the max value of concentration in front of dendrite are studied by analyzing concentration distribution along [100] direction to research the effect of supercooling temperature on microsegregation.

Figure 2 shows the concentration distribution along [100] direction at t=34200Δt with the melt inflow velocity of 1.3 m/s. Curves 1, 2 and 3 show the Cu concentration distributions for melt with flow from dendrite centre and along directions of upstream dendrite, normal to flow dendrite and downstream dendrite at t=34200Δt, respectively. Curve 0 shows Cu concentration distribution at the same solidification time for melt without flow. δ_1, δ_2 and δ_3 are the thickness values of concentration boundary layer in front of upstream dendrite, normal to flow dendrite and downstream dendrite, respectively. C_{L1}^*, C_{L2}^* and C_{L3}^* are the maximal concentrations in front of upstream dendrite, normal to flow dendrite and downstream dendrite, respectively. C_{S1}^*, C_{S2}^* and C_{S3}^* are the Cu concentrations in the centre of upstream dendrite, normal to flow dendrite and downstream dendrite primary dendrite arm, respectively. δ_0, C_{L0}^* and C_{S0}^* are the thickness values of concentration boundary layer in front of dendrite, the max concentration in front of dendrite tip and Cu concentration in the centre of dendrite for melt without flow, respectively.

4.1 Effect of melt forced lamina flow on thickness of concentration boundary layer

Figure 2 indicates that forced lamina flow can affect the thickness of dendrite tip concentration boundary layer. Figure 3 shows the relationship of concentration

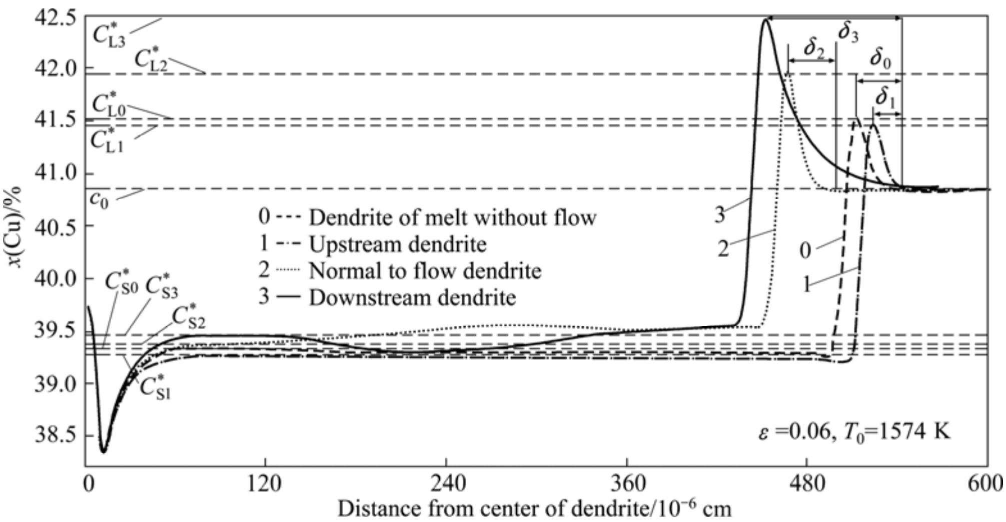

Fig. 2 Concentration distribution at t=34200Δt for melt with flow velocity u=1.3 m/s

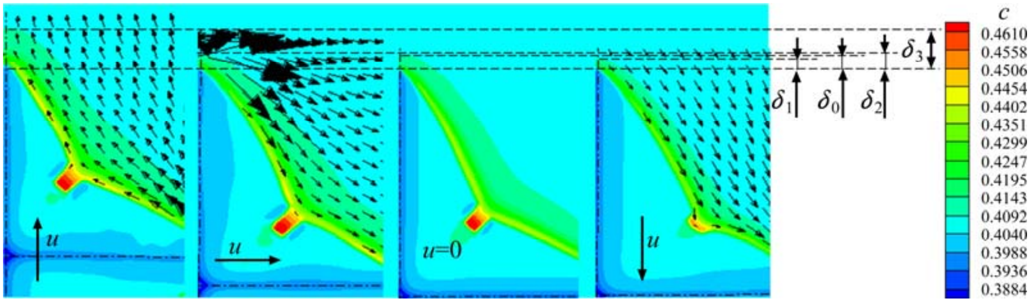

Fig. 3 Relationship of concentration boundary thickness in front of dendrite tip on supercooled melt in different flow directions

boundary thickness in front of the dendrite tip. There is a thickness of concentration boundary layer and in which only mass transfers in liquid−solid interface for melt with flow. What is more, mass transfer in the whole system is caused not only by diffusion but also by convection. At upstream dendrite, Cu atoms precipitated from solid phase do not enrich easily because of severe convection and diffusion. So, the thickness of concentration boundary layer for melt with flow is thinner than that without flow, namely, $\delta_1<\delta_0$. Convection is strong in upstream side normal to flow dendrite, which is the same as that in the upstream of the dendrite. But in the downstream side normal to flow dendrite, convection is weak because of asylum of dendrite arm, and Cu is diffused away hardly. The two factors cause that the thickness of concentration boundary layer in front of normal to flow dendrite tip is thicker than that without flow, namely, $\delta_2>\delta_0$. In the downstream side of dendrite, convection is weaker than everywhere of the asylum of dendrite arm. Cu is precipitated not only from solid phase but also from the upstream of dendrite and cumulates here. So the thickness of concentration boundary layer is thicker here than that in front of normal to flow dendrite tip, namely, $\delta_3>\delta_2$. In all, the thickness relationship of concentration boundary layer in front of dendrite tip in 3 directions for melt with and without flow is shown as

$$\delta_1<\delta_0<\delta_2<\delta_3 \tag{11}$$

4.2 Effect of melt forced lamina flow on maximal value of concentration in front of dendrite tip

Melt forced lamina flow has an effect on the maximal Cu concentration in front of dendrite tip. The same as previous analysis, the strongest convection happens in front of upstream dendrite tip. Cu precipitated from solid phase diffuses away easily and cannot hinder concentration. As a result, the concentration of Cu is lower for melt with flow than without flow. As shown in Fig. 2, there is $c^*_{\mathrm{L0}} > c^*_{\mathrm{L1}}$. Convection is strong in the upstream side of normal to flow dendrite but weak in the downstream side. So, Cu atoms accumulate and their maximal concentration is higher than that without flow, as shown in Fig. 2. The relationship is $c^*_{\mathrm{L2}} > c^*_{\mathrm{L0}}$. In the downstream side of dendrite, Cu hardly diffuses away because convection is weak. What is more, Cu atoms from dendritic upside with melt flow accumulate there. So, Cu enriches seriously, and the concentration is the highest, namely, $c^*_{\mathrm{L3}} > c^*_{\mathrm{L2}}$. In all, the maximal concentration relationship in front of dendrite tip in 3 directions for melt with flow and without flow is shown as:

$$c^*_{\mathrm{L3}} > c^*_{\mathrm{L2}} > c^*_{\mathrm{L0}} > c^*_{\mathrm{L1}} \tag{12}$$

4.3 Effect of melt forced lamina flow on microsegregation

Figure 1(c) shows that there is microsegregation within dendrite arms. Poor Cu domain occurs in the axis center of primary dendrite arm which is caused by the dendrite tip curvature radius. By comparing Fig. 1(c) with Fig. 1(f), microsegregation exists with new features for melt with flow. Figure 4 shows that in 2D simulation, the length and half width of poor Cu domain are l_0 and w_0 in primary dendrite arm for melt without flow. For melt with flow, the length and half width of poor Cu domain are l_1 and w_1 in the upstream dendrite, respectively, and

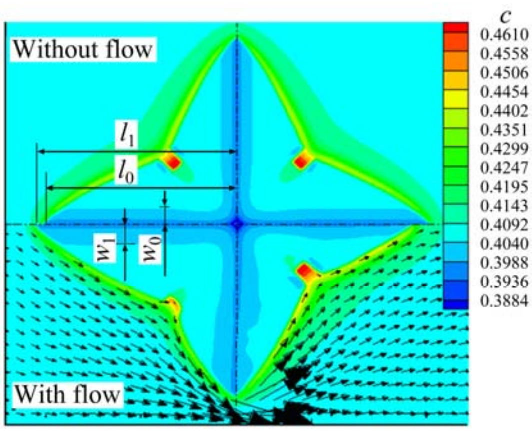

Fig. 4 Comparison of microsegregation between melt without flow and with flow

$$l_1>l_0,\ w_1>w_0 \tag{13}$$

It is shown that the area of poor Cu domain increases in upstream dendrite for melt with flow. Because the thickness of concentration boundary layer is thinner, the concentration gradient is larger and the maximal concentration in front of upstream tip is smaller for melt with flow. Those factors are propitious to constitutional supercooling. As a result, the upstream dendrite growth velocity and curvature radius increase. So, the area of poor Cu domain increases.

2) For the melt with flow, after solidification speed becomes stable, Cu concentration is different in the axis center of 3-direction primary dendrite arms, as shown in Fig. 2. Cu concentration in the axis center of upstream dendrite is lower for melt with flow than that without flow, namely, $c_{S1}^{*} < c_{S0}^{*}$. However, Cu concentration in axis center of downstream dendrite (c_{S3}^{*}) and normal to flow dendrite (c_{S2}^{*}) is higher for melt with flow than without flow. Flow state fluctuate is caused by dendritic morphology growth, and c_{S3}^{*} fluctuate is caused by flow state. But the relationship $c_{S3}^{*} > c_{S2}^{*} > c_{S0}^{*}$ still exists. This is because the local equilibrium state of concentration in solid and liquid phase always exists. The ratio of concentration in solid phase side (c_{S}^{*}) and liquid phase side (c_{L}^{*}) around the interface is corresponded to the solute equilibrium partition coefficient K_0 whether the solute accumulation is high or low.

$$K_0 = \frac{c_S^*}{c_L^*} \tag{14}$$

that is

$$c_S^* = K_0 c_L^* \tag{15}$$

Combining Eqs. (12) and (15) obtains

$$c_{S3}^* > c_{S2}^* > c_{S0}^* > c_{S1}^* \tag{16}$$

The simulation results are coupled with theoretical analysis results based on the solidification theory.

The plasticity, toughness and tensile properties of the alloy degrade because of microsegregation. In order to eliminate microsegregation, one of the easiest ways is homogenization for a long time to cast alloy at lower temperature than the solidus temperature.

5 Conclusions

1) Supercooled melt forced lamina flow can affect the thickness of concentration boundary layer and the max concentration in front of dendrite tip, the relationships are $\delta_1<\delta_0<\delta_2<\delta_3$ and $c_{L3}^* > c_{L2}^* > c_{L0}^* > c_{L1}^*$, respectively.

2) Because of melt flow, solute enrichment is weakened at upstream dendrite. But in downstream dendrite, enrichment is severe and the risk of shrinkage cavity occurrence increases.

3) Microsegregation is complex in primary dendrite arm for melt with flow. The concentration follows the relationship of $c_{S3}^* > c_{S2}^* > c_{S0}^* > c_{S1}^*$. 2D simulation results show that the area of poor Cu domain is lager inside of upstream dendrite. Homogenization should be done after solidification at temperature lower than the solidus temperature to eliminate microsegregation.

References

[1] DUAN Meng-meng, CHENG Chang-le, LI Zhan-yao, JIN Quan-wei. The effect of buoyancy driven convection on interface topography during solidification process [J]. Science in China G, 2007, 37(3): 396−402. (in Chinese)

[2] QIU Wen-xu, CHEN Chang-le, MA Qiang, DONG Hui-ying, ZHANG Li-xue, JIA Xi-wen. Influence of solute gradient in the dendritic growth of binary alloy [J]. Materials Science and Technology, 2010, 18(5): 635−643. (in Chinese)

[3] XUE Qiang, LI Hong-wei. Influence of pressure on shrinkage porosity prediction [J]. The Chinese Journal of Nonferrous Metals, 2005, 15(2): 217−221. (in Chinese)

[4] BECKERMANN C, DIEPERS H J, STEINBACH I, KARMA A, TONG X. Modeling melt convection in phase-field simulations of solidification [J]. Journal of Computational Physics, 1999, 154(2): 468−496.

[5] SUN Y, BECKERMANN C. Effect of solid-liquid density change on dendrite tip velocity and shape selection [J]. Journal of Crystal Growth, 2009, 311(4): 4447−4453.

[6] TONG X, BECKERMANN C, KARMA A, LI Q. Phase-filed simulations of dendritic crystal growth in forced flow [J]. Phys Rev E, 2001, 63: 061601-1−16.

[7] ZHU Ming-fang, DAI Ting, LI Cheng-yun, HONG Jun-shao. Numerically simulation the dendritic growth process under forced flow [J]. Science in China E, 2005, 35(7): 673−687. (in Chinese)

[8] KARMA A, RAPPEL W J. Quantitative phase-field modeling of dendritic growth in two and three dimensions [J]. Physical Review Letter E, 1998, 57(4): 4324−4349.

[9] JEONG J H, DANTZIG J A, GOLDENFELD N. Dendritic growth with fluid flow in pure materials [J]. Metallurgical and Material Transaction A, 2003, 34(3): 459−466.

[10] BOETTINGER W J, WARREN J A, BECKERMANN C, KARMA A. Phase-field simulation of solidification [J]. Annual Review of Material Research, 2002, 32(8): 163−194.

[11] ZHU Yao-chan, YANG Gen-cang, WANG Jin-cheng, ZHAO Da-wen, FAN Jian-feng. Multi-phase field simulation of unidirectional solidification for binary eutectic alloys [J]. The Chinese Journal of Nonferrous Metals, 2005, 15(7): 1026−1032. (in Chinese)

[12] CEHN Yun, KANG Xiu-hong, LI Dian-zhong. Phase-field modeling of free dendritic growth with adaptive finite element method [J]. Acta Physica Sinica, 2009, 58(1): 390−398. (in Chinese)

[13] TONG X, BECKERMANN C, KARMA A. Velocity and shape selection of dendritic crystals in a forced flow [J]. Physical Review Letter E, 2000, 61(1): 49−52.

[14] FRIEDRICH H, SCHUMANN S. Research for a “new age of magnesium” in the automotive industry [J]. Journal of Materials Processing Technology, 2001, 117(3): 276−281.

[15] NARSKI J, PICASSO M. Adaptive 3D finite elements with high aspect ratio for dendritic growth of a binary alloy including fluid flow induced by shrinkage [J]. Fluid Dynamics and Materials

Processing, 2007, 3(1): 49−64.
[16] LAN C W, SHIH C J. Phase field simulation of non-isothermal free dendritic growth of a binary alloy in a forced flow [J]. Journal of Crystal Growth, 2004, 264(3): 472−482.
[17] YUAN Xun-feng, DING Yu-tian, GUO Ting-biao, HU Yong, TANG Xiang-qian. Numerical simulation of dendritic growth of magnesium alloys using phase-field method under forced flow [J]. The Chinese Journal of Nonferrous Metals, 2010, 20(8): 1474−1480. (in Chinese)
[18] LONG Wen-yuan, CAI Qi-zhou, CHEN Li-liang, WEI Bo-kang. Phase-field simulations of solidification of Al-Cu binary alloys [J]. The Chinese Journal of Nonferrous Metals, 2004, 14(2): 291−296. (in Chinese)
[19] ZHU Chang-sheng, XIAO Rong-zhen, WANG Zhi-ping, FENG Li. Numerical simulation of recalescence of 3-dimensional isothermal solidification for binary alloy using phase-field approach [J]. The Chinese Journal of Nonferrous Metals, 2009, 19(6): 1286−1293. (in Chinese)
[20] CHEN Yu-juan, CHEN Chang-le. Simulation of the influence of convection velocity on upstream dendritic growth using phase-field method [J]. Acta Physica Sinica, 2008, 57(7): 4585−4589. (in Chinese)
[21] LONG Wen-yuan, LV Dong-lan, XIA Chun, PAN Mei-man, CAI Qi-zhou, CHEN Li-liang. Phase-field simulation of non-isothermal solidification dendrite growth of binary alloy under the force flow [J]. Acta Physica Sinica, 2009, 58(11): 7802−7808. (in Chinese)
[22] WANG Zhi-ping, WANG Jun-wei, ZHU Chang-sheng, FENG Li, XIAO Rong-zhen. Phase-field simulation of pure material dendritic growth based on sola algorithm in force laminar flow [J]. Journal of Mechanical Engineering, 2010, 46(14): 60−67. (in Chinese)
[23] ANZAI K. Introduction to fluid flow simulation [J]. Light Metal, 1994, 44(1): 57−66. (in Japanese)

相场法定量模拟强迫层流对微观偏析的影响

王军伟[1], 王智平[1,2], 路 阳[1,2], 朱昌盛[1,3], 冯 力[1], 肖荣振[1]

1. 兰州理工大学 甘肃省有色金属新材料重点实验室，兰州 730050；
2. 甘肃省有色金属及复合材料工程研究中心，兰州 730050；
3. 兰州理工大学 CAD 中心，兰州 730050

摘　要：采用耦合流场的相场模型，模拟 Ni−Cu 合金过冷熔体流动对液固界面前沿浓度分布的影响；定量分析强迫层流对迎流方向、垂直流动方向与逆流方向枝晶尖端前沿浓度边界层厚度，浓度最大值和枝晶微观偏析的影响。结果表明：溶质场和流场二者相互影响；枝晶上游侧浓度边界层的厚度较薄，溶质浓度的最大值较小；而枝晶下游侧恰好与此相反。贫 Cu 区域在迎流方向枝晶臂沿枝晶轴线方向的宽度较大，但 Cu 原子的浓度较低，微观偏析最严重，枝晶下游侧缩松倾向加剧。

关键词：计算机模拟；相场法；凝固；强迫层流；微观偏析；溶质再分配；缩松

(Edited by FANG Jing-hua)